

Random-access quantum memory using chirped pulse phase encoding

James O’Sullivan,^{1,*} Oscar W. Kennedy,^{1,*} Kamanasish Debnath,² Joseph Alexander,¹
 Christoph W. Zollitsch,¹ Mantas Šimėnas,¹ Akel Hashim,^{3,4} Christopher N. Thomas,⁵
 Stafford Withington,⁵ Irfan Siddiqi,^{3,4} Klaus Mølmer,² and John J. L. Morton^{1,6}

¹*London Centre for Nanotechnology, UCL, 17-19 Gordon Street, London, WC1H 0AH, UK*

²*Department of Physics and Astronomy, Aarhus University, DK-8000 Aarhus C, Denmark*

³*Quantum Nanoelectronics Laboratory, Department of Physics, UC Berkeley, California 94720, USA*

⁴*Lawrence Berkeley National Laboratory, Berkeley, CA 94720, USA*

⁵*Cavendish Laboratory, University of Cambridge, JJ Thomson Ave, Cambridge CB3 0HE, UK*

⁶*Department of Electrical and Electronic Engineering, UCL, Malet Place, London, WC1E 7JE, UK*

As in conventional computing, key attributes of quantum memories are high storage density and, crucially, random access, or the ability to read from or write to an arbitrarily chosen register. However, achieving such random access with quantum memories in a dense, hardware-efficient manner remains a challenge, for example requiring dedicated cavities per qubit or pulsed field gradients. Here we introduce a protocol using chirped pulses to encode qubits within an ensemble of quantum two-level systems, offering both random access and naturally supporting dynamical decoupling to enhance the memory lifetime. We demonstrate the protocol in the microwave regime using donor spins in silicon coupled to a superconducting cavity, storing up to four multi-photon microwave pulses in distinct memory modes and retrieving them on-demand up to 2 ms later. A further advantage is the natural suppression of superradiant echo emission, which we show is critical when approaching unit cooperativity. This approach offers the potential for microwave random access quantum memories with lifetimes exceeding seconds, while the chirped pulse phase encoding could also be applied in the optical regime to enhance quantum repeaters and networks.

Quantum memories (QMs) capable of faithfully storing and recalling quantum states on-demand are powerful ingredients in building quantum networks [1] and quantum information processors [2]. Ensembles of quantum systems are natural platforms for QMs, given their large storage capacity. Multiple qubits can be stored taking advantage of direct spatial addressing to access different regions of the ensemble [2, 3]. However, for ensembles in the solid state that offer prospects for high-density QMs and typically have inhomogeneous broadening, *spectral*-addressing can be used to distinguish excitations stored collectively in the ensemble. Solid-state atomic ensembles have long coherence times for both microwave [5–9] and optical [8–10] transitions and can couple to resonant cavities facilitating read, write and control operations. Coherent control allows coherence times to be extended by dynamical decoupling (DD) techniques [9, 11–13] or to transfer the qubit state to a basis with longer coherence [14]. Coupling the ensemble to the cavity either in the strong coupling regime [15–19] or with cooperativity $C = 1$ facilitates writing and reading information into and out of the ensemble with unit efficiency [20, 21].

A simple widely used memory protocol is the Hahn echo [22], where an input excitation stored within an ensemble is inverted by a π pulse and re-emitted later as an ‘echo’. This has been used widely in multimode microwave [6, 23, 24] and optical [25, 26] memories and formed the basis of early (classical) information storage proposals [27]. The Hahn echo approach is unsuitable for QMs, leading to amplified (and thus noisy) emission from quantum systems in their excited state [28]. One

solution is to use two π pulses to return the ensemble predominantly to the ground state [21, 29], which requires suppressing the emission of the echo that would otherwise appear after the first π pulse. The Hahn echo sequence is a ‘first-in last-out’ memory, rather than permitting random access to stored qubits. Various approaches have been explored to address these limitations: frequency-tunable cavities [30] can be shifted off-resonance to suppress unwanted echoes; external electric or magnetic field gradients can be used to label stored excitations [31]; and AC Stark shifts can shift the emission of excitations into different time bins [32]. None of these ingredients alone realises a random access QM and the requirement of additional control fields poses a significant practical limitation. For example, the magnetic field gradients used in Ref. [4] to retrieve two microwave excitations in arbitrary order have poor compatibility with the superconducting resonators and qubits used to achieve high-cooperativity and provide the quantum states to be stored respectively. In this Letter we present a simpler and more powerful approach to labelling and recalling stored qubits from an ensemble QM, using chirped control pulses. This protocol suppresses unwanted echoes, allows random access to multiple memory modes with read and write operations performed in arbitrary order, and naturally embeds DD. We demonstrate the performance of the protocol using weak microwave excitations stored within donor spins in silicon.

Sweeping the frequency of a control pulse across an atomic transition can be used to perform an inversion (or π pulse) by ‘adiabatic fast passage’ (AFP). Chirped

pulses — e.g. wideband, uniform rate smooth truncation (WURST) — have multiple advantages for control of ensemble QMs. First, their robustness to variations in the strength of the control field (e.g. laser field or microwave magnetic field) — particularly attractive for planar microresonators where the coupling is often highly inhomogeneous [33]. Second, when used to refocus an inhomogeneously broadened ensemble, a *pair* of pulses must be applied to produce an echo and suppression of the first echo is an inherent feature as has been demonstrated in the optical domain [29, 34, 35], and is shown in Fig. 1(a). Third (explored in detail below) is that the chirped pulse can be used to imprint a pulse-specific phase distribution across the atomic ensemble, allowing multiple excitations to be independently stored and retrieved within the ensemble QM.

Our experiments are performed on an ensemble of bismuth donor spins in a natural silicon host, coupled to a superconducting niobium microwave cavity at 100 mK with resonant frequency 7.093 GHz and quality factor $\sim 18,000$ details in supplementary information (SI) Fig. S2. Figure 1(a) shows two WURST π -pulses refocussing a microwave excitation and confirms that *two* such pulses are required to observe an echo, as illustrated schematically in Fig. 1(b). The inhomogeneous ensemble can be decomposed into sub-ensembles with spin transition frequency detuning δ and spin-cavity coupling g_0 . Precession of the sub-ensembles over some time τ (the ‘dephasing’ period) causes the excitation to evolve into a spin wave with wavevector k_δ in spin-detuning. The WURST ‘ π -pulse’ inverts the phase acquired by the spins, and imparts some additional phase shift ϕ_W , that varies across the sub-ensemble parameters δ and g_0 , and which is a function of WURST parameters (chirp rate and pulse amplitude). Following a subsequent ‘rephasing’ period of τ , the spin wave defined by k_δ is refocused, however, due to the phase pattern defined by ϕ_W , there is no ensemble coherence and no collective emission of an echo. A second *identical* WURST pulse applied later unwinds the phase pattern ϕ_W , so that when k_δ next returns to 0, the initial excitation is emitted as an echo. The phase patterns $\phi_{W,i}$, defined by different WURST pulses, equivalently the modes of the memory, provide the storage index which we exploit in our chirped-pulse QM protocol, as shown in Fig. 1(c). The application of a WURST pulse before and after an excitation, ‘writes’ it into the ensemble without affecting previously written excitations. Applying the same pair of WURST pulses later reads out the excitation, thus enabling random access of the QM. By applying WURST pulses in identical pairs, we ensure that excitations already in the memory are unaffected by any read/write operation, beyond experiencing periodic inversions that assist in mitigating noise. The requirements of the WURST pulses to achieve independent storage modes are presented further below.

We illustrate the importance of suppressing echo emis-

sion from an inverted ensemble (Fig. 2). Applying N_{inv} WURST π -pulses (for $N_{\text{inv}}=0-3$) before an echo sequence Fig. 2(a), prepares the ensemble in the ground (N_{inv} even) or inverted (N_{inv} odd) state. Using weak excitations of $\langle n \rangle \sim 200$ microwave photons ensures that the ensemble is only weakly perturbed from prepared state when emitting. Figure 2(c) shows that echoes emitted from an inverted ensemble have larger amplitude than those emitted from a (quasi-)ground state ensemble, further supported by the dependence on the parity of N_{inv} seen in Fig. 2(d). These observations indicate there has been amplification of the input signal from stimulated emission (the emitted echo is always weaker than the input signal due to other losses).

By increasing the delay time between the WURST pulses, we measure a coherence lifetime of this memory, $T_2 \sim 0.6$ ms (SI Fig. S3). This lifetime can be extended using DD sequences consisting of repeated π -pulses [13, 36]. Using identical WURST pulses, an echo is emitted after every two pulses (see Fig. 2). Introducing a second WURST pulse (‘B’) of different chirp rate and/or pulse amplitude to the first (‘A’), we apply the sequence $A[BB]_nA$ following the initial excitation. An echo only appears after the second ‘A’ pulse is applied, thus suppressing repeated emission during the DD. The resulting coherence decays are longer, and provides a measure of the memory storage lifetime, $T_M = 2.0(2)$ ms.

The $A[AA]_nA$ WURST DD sequence (in which an echo is emitted after each pair of π pulses) gives a decay time constant which is shorter than T_M . We model this behaviour assuming a constant fraction η_{em} of the excitation is lost with each echo, in addition to exponential decay with time constant T_M . A fit to the data yields $\eta_{\text{em}} = 0.17(7)$ — interpreting this value as the one-way efficiency, it can be related to the cooperativity by $\eta_{\text{em}} = \frac{4C}{(1+C)^2}$ (see Ref [20]) giving $C = 0.05(2)$, in good agreement with $C = 0.07(2)$ extracted from fitting to S-parameter measurements of the cavity frequency and linewidth [37] (see SI). This one-way efficiency is larger than previously reported values for microwave QMs of 0.01–0.043 [6, 23, 24] due to the higher cooperativity in this sample. In a high efficiency QM ($C \sim \eta_{\text{em}} \sim 1$), DD sequences of this type will be essential to avoid the stored excitation being emitted prematurely.

Having demonstrated the ability to control echo emission using chirped pulses, we now show an experimental demonstration of the QM protocol introduced in Fig. 1(c). The protocol is composed of repeating blocks of the form $(\pi_j - \square - \pi_j)$ where π_j is a unique WURST π -pulse whose parameters (chirp rate and amplitude) address a particular storage index j , and \square can be i) a weak input excitation to be stored in location j of the memory; ii) an echo, constituting an excitation being retrieved from location j in memory; or iii) null, for a clock cycle in which no information is being read or written. The null case is used for DD to preserve the quantum

information already stored with π_j addressing an unused memory mode. Figure 3 (a) demonstrates the operation of this random access protocol through the storage, protection and retrieval of four weak ($\langle n \rangle \sim 1200$ photon) microwave excitations, using five distinct WURST pulses with varying chirp rates (see Fig. 3 (b)). Photon number is calibrated from measurements of Rabi frequency and Purcell relaxation (SIFig. S2).

Each of the four initial excitations is encoded into the memory using a pair of identical WURST pulses (colour-coded in teal, coral, lime and mustard), and retrieved some time later (varying from 0.5 to 2.5 ms for the different excitations) by applying the same pair of pulses. Each of the four echoes can be unambiguously matched to one of the original excitations through their phase (see Fig. 3 (c)), which we further confirm by repeating the sequence with only one of the four excitations present (SIFig. S10). A fifth variant of WURST pulse (shown in grey) is used in the sequence to perform DD. The amplitudes of the retrieved signals are reduced compared to the input states due to the finite efficiency of the memory resulting from the limited cooperativity in these experiments. We therefore re-scale the echo amplitudes by the factors (3–31) shown in Fig. 3 (c) and observe that the phase of the excitation is generally well preserved. The largest phase error, from the second excitation (coral) may be partly attributed to a phase shift from the Josephson parametric amplifier, as the echo is of larger amplitude due to the short storage time (SIFig. S4).

The capacity of the QM is determined by the number of independent WURST pulses that can be used in the protocol. This can be related to the spectral width (Δ_f) of the ensemble used for storage, equal to the narrower of the cavity linewidth κ or that of the inhomogeneous ensemble. The WURST pulses can be parameterised using their chirp rate R and their amplitude A_W ($A_W = 1$ gives Rabi frequency $\Omega = 2.87$ MHz), bounds illustrated in Fig. 4. A_W has a lower bound from the requirement of adiabaticity [38], and some upper bound set by the max pulse amplitude (limited by the pulse amplifier in our setup, or in general, heating of the sample due to the pulses). We determined the adiabatic bounds on A_W in our experiment through microwave simulations, confirmed through echo experiments of the type illustrated in Fig. 1(a) (SIFig. S6). R has some upper bound set by the experimental frequency resolution and a lower bound determined by the need to at least chirp across Δ_f within the effective duration of the WURST pulse ($T_{W,\text{eff}}$), such that $R \gg \Delta_f/T_{W,\text{eff}}$.

The separation of distinct pulses in R and A_W is governed by the requirement of independence in the storage modes of the memory. We explore this using pulse sequences of the form $\alpha - \pi_A - \pi_B - [\text{echo}]$, where an excitation α is followed by two WURST pulses whose parameters are varied. For sufficiently distinct π_A and

π_B , no echo should be observed. First, we fix the parameters of π_A and vary those of π_B , as shown in the inset of Fig. 4. Equivalent WURST pulses lie on lines of positive gradient — as R increases, the phase from the WURST pulse decreases, compensated by increasing A_W . Additional two-dimensional parameter sweeps are shown as green lines in Fig. 4, we also acquire several one-dimensional sweeps (a subset are shown in Fig. 4). We extract the different regions of WURST pulses equivalence requiring that each WURST pulse is separated by at least the half width, *hundredth* max of the neighbouring regions (SIFig. S7). We find ~ 8 distinct WURST pulses at an amplitude of 0.6 V, with an equal number of WURST pulses when chirping in the reverse direction, giving ~ 16 distinct memory modes. Chirped pulse encoding can be combined with other methods such as time-bin encoding (used to store up to 100 weak microwave excitations [4, 6]) to implement a memory offering random access to large quantum registers. We illustrate the principle using a 5-excitation register in the SIFig. S9. The storage capacity could be increased by addressing the instrumentation-limited bounds on R and A_W , and by increasing the WURST pulse duration (at the expense of slower read/write speeds and less effective DD). Approaches to increase the cooperativity to ~ 1 in this system include increasing the spin-cavity coupling g_0 and the number of resonant spins [39]. Coherence times over 300 ms have been shown for near-surface Bi donors in isotopically enriched ^{28}Si [6].

This chirped pulse protocol could also be applied to provide random read/write access in optical QMs. Chirped microwave pulses could be applied to directly drive transitions in spin-active optical QMs, such as Nd in yttrium orthovanadate [32], providing DD and controlling access to a register of stored optical excitations. Furthermore, adiabatic fast passages (achieved using acousto-optic and electro-optic modulators) have been used to optimally invert optical transitions in demonstrations of optical QMs [29]. Similarly chirped optical pulses of varying parameters could allow for a random access protocol to be directly implemented in the optical domain, taking advantage of the stronger atom-cavity coupling and larger cavity bandwidth.

ACKNOWLEDGEMENTS

We thank Philippe Goldner for insightful discussions relating to the implementation of this protocol in the optical domain. We thank the UK National Ion Beam Centre (UKNIBC) where the silicon samples were ion implanted and Nianhua Peng who performed the ion implantation. This work has received funding from the U.K. Engineering and Physical Sciences Research Council (EPSRC), through UCLQ postdoctoral fellowships (O.W.K, M.S.) Grant No. EP/P510270/1 and a Doc-

toral Training Grant (J.O'S.). J.J.L.M. acknowledges funding from the European Research Council under the European Union's Horizon 2020 research and innovation programme (Grant agreement No. 771493 (LOQOMOTIONS)).

AUTHOR CONTRIBUTIONS

J.O'S and O.W.K. performed the experiments with assistance from C.W.Z.. J.O'S, O.W.K. and J.J.L.M. analysed the data with input from J.A. and M.S.. J.A. and J.J.L.M. designed the random access protocol with input from O.W.K. and J.O'S. K.D. and K.M. performed numerical analyses and the analytical treatment. C.T. and S.W. fabricated the device. A.H. and I.S. assembled, tested, and provided scientific support in the operation of the JPA. J.O'S, O.W.K. and J.J.L.M. wrote the manuscript with input from all authors.

DATA AVAILABILITY

The datasets generated and analysed during the current study are available in the UCL Research Data repository, doi.org/10.5522/04/14541747.

* These authors have contributed equally to this work

- [1] H. J. Kimble, *Nature* **453**, 1023 (2008).
- [2] M. Mariani, H. Wang, T. Yamamoto, M. Neeley, R. C. Bialczak, Y. Chen, M. Lenander, E. Lucero, A. D. O'Connell, D. Sank, *et al.*, *Science* **334**, 61 (2011).
- [3] N. Jiang, Y.-F. Pu, W. Chang, C. Li, S. Zhang, and L.-M. Duan, *npj Quantum Information* **5**, 1 (2019).
- [4] H. Wu, R. E. George, J. H. Wesenberg, K. Mølmer, D. I. Schuster, R. J. Schoelkopf, K. M. Itoh, A. Ardavan, J. J. Morton, and G. A. D. Briggs, *Physical Review Letters* **105**, 140503 (2010).
- [5] G. Wolfowicz, A. M. Tyryshkin, R. E. George, H. Riemann, N. V. Abrosimov, P. Becker, H.-J. Pohl, M. L. Thewalt, S. A. Lyon, and J. J. Morton, *Nature Nanotechnology* **8**, 561 (2013).
- [6] V. Ranjan, J. O'Sullivan, E. Albertinale, B. Albanese, T. Chanelière, T. Schenkel, D. Vion, D. Esteve, E. Flurin, J. Morton, and P. Bertet, *Physical Review Letters* **125**, 210505 (2020).
- [7] M. Steger, K. Saeedi, M. Thewalt, J. Morton, H. Riemann, N. Abrosimov, P. Becker, and H.-J. Pohl, *Science* **336**, 1280 (2012).
- [8] A. Ortu, A. Tiranov, S. Welinski, F. Fröwis, N. Gisin, A. Ferrier, P. Goldner, and M. Afzelius, *Nature Materials* **17**, 671 (2018).
- [9] N. Bar-Gill, L. M. Pham, A. Jarmola, D. Budker, and R. L. Walsworth, *Nature Communications* **4**, 1 (2013).
- [10] D. D. Sukachev, A. Sipahigil, C. T. Nguyen, M. K. Bhaskar, R. E. Evans, F. Jelezko, and M. D. Lukin, *Physical Review Letters* **119**, 223602 (2017).
- [11] B. Naydenov, F. Dolde, L. T. Hall, C. Shin, H. Fedder, L. C. Hollenberg, F. Jelezko, and J. Wrachtrup, *Physical Review B* **83**, 081201 (2011).
- [12] H. Y. Carr and E. M. Purcell, *Physical Review* **94**, 630 (1954).
- [13] S. Meiboom and D. Gill, *Review of Scientific Instruments* **29**, 688 (1958).
- [14] J. J. Morton, A. M. Tyryshkin, R. M. Brown, S. Shankar, B. W. Lovett, A. Ardavan, T. Schenkel, E. E. Haller, J. W. Ager, and S. Lyon, *Nature* **455**, 1085 (2008).
- [15] Y. Kubo, F. Ong, P. Bertet, D. Vion, V. Jacques, D. Zheng, A. Dréau, J.-F. Roch, A. Auffèves, F. Jelezko, *et al.*, *Physical Review Letters* **105**, 140502 (2010).
- [16] S. Weichselbaumer, M. Zens, C. W. Zollitsch, M. S. Brandt, S. Rotter, R. Gross, and H. Huebl, *Physical Review Letters* **125**, 137701 (2020).
- [17] S. Probst, H. Rotzinger, S. Wünsch, P. Jung, M. Jerger, M. Siegel, A. Ustinov, and P. Bushev, *Physical Review Letters* **110**, 157001 (2013).
- [18] D. Schuster, A. Sears, E. Ginossar, L. DiCarlo, L. Frunzio, J. Morton, H. Wu, G. Briggs, B. Buckley, D. Awschalom, *et al.*, *Physical Review Letters* **105**, 140501 (2010).
- [19] T. Zhong, J. M. Kindem, J. Rochman, and A. Faraon, *Nature Communications* **8**, 1 (2017).
- [20] M. Afzelius, N. Sangouard, G. Johansson, M. Staudt, and C. Wilson, *New Journal of Physics* **15**, 065008 (2013).
- [21] B. Julsgaard, C. Grezes, P. Bertet, and K. Mølmer, *Physical Review Letters* **110**, 250503 (2013).
- [22] E. L. Hahn, *Physical Review* **80**, 580 (1950).
- [23] S. Probst, H. Rotzinger, A. Ustinov, and P. Bushev, *Physical Review B* **92**, 014421 (2015).
- [24] C. Grezes, B. Julsgaard, Y. Kubo, M. Stern, T. Umeda, J. Isoya, H. Sumiya, H. Abe, S. Onoda, T. Ohshima, *et al.*, *Physical Review X* **4**, 021049 (2014).
- [25] M. Lovrić, D. Suter, A. Ferrier, and P. Goldner, *Physical Review Letters* **111**, 020503 (2013).
- [26] A. I. Lvovsky, B. C. Sanders, and W. Tittel, *Nature Photonics* **3**, 706 (2009).
- [27] A. Anderson, R. Garwin, E. Hahn, J. Horton, G. Tucker, and R. Walker, *Journal of Applied Physics* **26**, 1324 (1955).
- [28] J. Ruggiero, J.-L. Le Gouët, C. Simon, and T. Chanelière, *Physical Review A* **79**, 053851 (2009).
- [29] V. Damon, M. Bonarota, A. Louchet-Chauvet, T. Chanelière, and J.-L. Le Gouët, *New Journal of Physics* **13**, 093031 (2011).
- [30] Y. Kubo, C. Grezes, A. Dewes, T. Umeda, J. Isoya, H. Sumiya, N. Morishita, H. Abe, S. Onoda, T. Ohshima, *et al.*, *Physical Review Letters* **107**, 220501 (2011).
- [31] B. Kraus, W. Tittel, N. Gisin, M. Nilsson, S. Kröll, and J. I. Cirac, *Physical Review A* **73**, 020302 (2006).
- [32] T. Zhong, J. M. Kindem, J. G. Bartholomew, J. Rochman, I. Craiciu, E. Miyazono, M. Bettinelli, E. Cavalli, V. Verma, S. W. Nam, *et al.*, *Science* **357**, 1392 (2017).
- [33] A. J. Sigillito, H. Malissa, A. M. Tyryshkin, H. Riemann, N. V. Abrosimov, P. Becker, H.-J. Pohl, M. L. Thewalt, K. M. Itoh, J. J. Morton, *et al.*, *Applied Physics Letters* **104**, 222407 (2014).
- [34] K. Gerasimov, M. Minnegaliev, S. Moiseev, R. Urmancheev, T. Chanelière, and A. Louchet-Chauvet, *Optics and Spectroscopy* **123**, 211 (2017).

- [35] M. Bonarota, J. Dajczgewand, A. Louchet-Chauvet, J.-L. Le Gouët, and T. Chanelière, *Laser Physics* **24**, 094003 (2014).
- [36] L. Viola, E. Knill, and S. Lloyd, *Physical Review Letters* **82**, 2417 (1999).
- [37] E. Abe, H. Wu, A. Ardavan, and J. J. Morton, *Applied Physics Letters* **98**, 251108 (2011).
- [38] A. Doll, S. Pribitzer, R. Tschaggelar, and G. Jeschke, *Journal of Magnetic Resonance* **230**, 27 (2013).
- [39] J. O’Sullivan, O. W. Kennedy, C. W. Zollitsch, M. Šimėnas, C. N. Thomas, L. V. Abdurakhimov, S. Withington, and J. J. Morton, *Physical Review Applied* **14**, 064050 (2020).

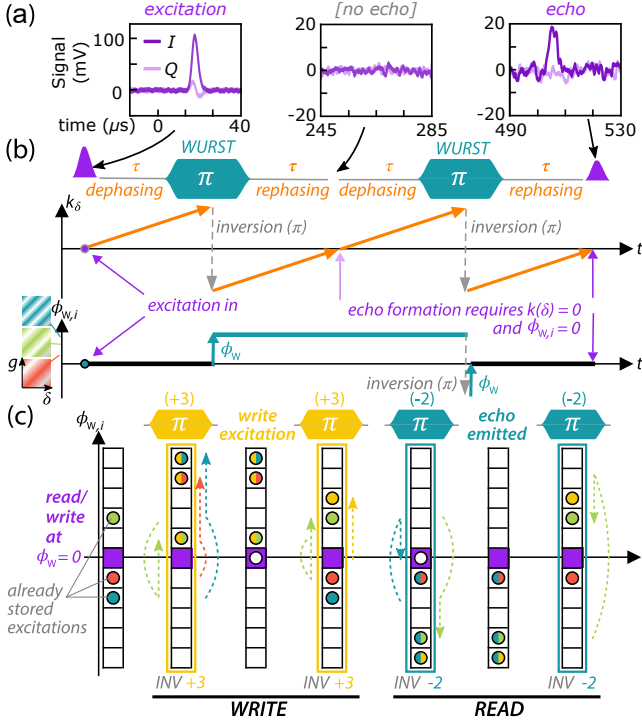


Figure 1. Using chirped pulses to silence echoes and encode quantum information. (a) A weak ($\langle n \rangle \sim 200$ photon) Gaussian microwave excitation is applied to an ensemble of Bi donor spins in silicon followed by two chirped ‘WURST’ π -pulses. A spin echo is observed only after the second WURST pulse. (b) The WURST pulse (index i) inverts the phase of the ensemble and imprints a phase pattern $\phi_{W,i}$ in the space of the atom-cavity coupling g_0 , and the frequency detuning δ . k_δ describes a wavevector of phase acquisition in frequency-space, which grows linearly in time by the precession of the inhomogeneously broadened ensemble. Excitations are stored in the ensemble at $k_\delta = \phi_W = 0$. A WURST pulse is applied at time τ , and a further τ after the pulse the spin-wave due to inhomogeneous broadening is refocused ($k_\delta = 0$), however, the WURST-imprinted phase pattern ϕ_W remains, suppressing echo emission. A further period of τ -WURST- τ returns the excitation to $\phi_W(g, \delta) = 0$ and an echo is emitted. (c) The function $\phi_{W,i}(g, \delta)$ is defined by the chirped pulse parameters, and can be used as a storage index to encode quantum excitations into the quantum memory. We illustrate WRITE and READ operations: Applying a WURST pulse (illustrative $\phi_{W,i}$ index: +3) before and after some excitation, it becomes stored within the corresponding region in ϕ_W -space leaving previously written excitations unaffected. The same procedure addressing a previously stored excitation causes it to be emitted as an echo.

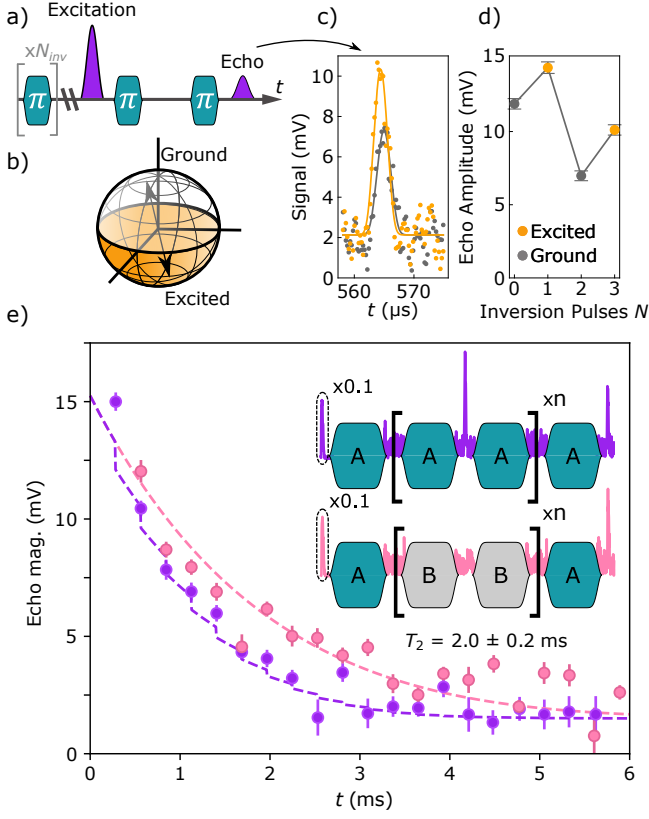


Figure 2. Demonstrating the importance of suppressed echo emission. (a) The pulse sequence used to study the echo following a pair of WURST pulses as a function of the state of the ensemble. (b) The approximate ensemble ground and excited state in a Bloch sphere representation of the ensemble magnetisation. (c) Two example echoes emitted from the ground state ($N_{inv} = 2$) or inverted state ($N_{inv} = 3$). Larger amplitude echoes are seen from the inverted ensembles due to amplification of the echo, which adds noise to a quantum memory. (d) Echo amplitude as a function of N_{inv} . The overall reduction of echo amplitude with increasing N_{inv} is likely due to gradual saturation of the spin ensemble. (e) Coherence decay rates from different WURST dynamical decoupling sequences. Given identical pulses ($A[AA]_nA$ - purple) echo emission occurs every second pulse leading to an accelerated decay in coherence compared to an $A[BB]_nA$ (pink) sequence where only one echo is emitted, at the end. A fit to the $A[BB]_nA$ data (dashed line) gives a coherence time of 2 ms, while fitting to the $A[AA]_nA$ data accounting for additional loss from repeated echoes (dashed line, see Eq. 5 SI) gives a memory efficiency η_{em} of 0.17. Error bars represent one standard deviation from fitting Gaussians to echoes.

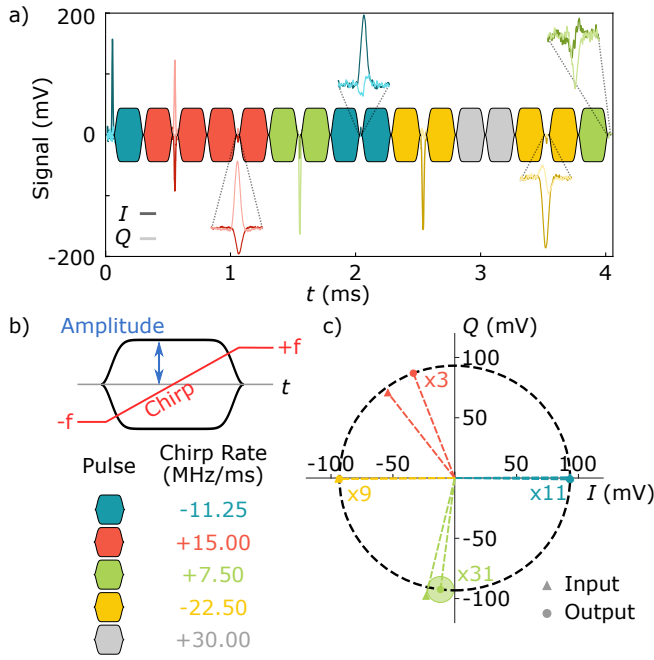


Figure 3. **The random access memory protocol.** (a) An example section of the memory protocol. WURST pulses, excitations and echoes are colour coded. Excitations and echoes are shown with magnified echoes offset from the main trace. In total four excitations are stored and storage times exceed 2 ms. The first and last pulses do not come in pairs as the memory sequence starts and finishes half way through a clock cycle. (b) The parameters of the WURST pulses used in (a). (c) Echoes and excitations on an Argand diagram matching their phases. The magnitude of each echo is rescaled to account for losses from dephasing and finite memory efficiency.

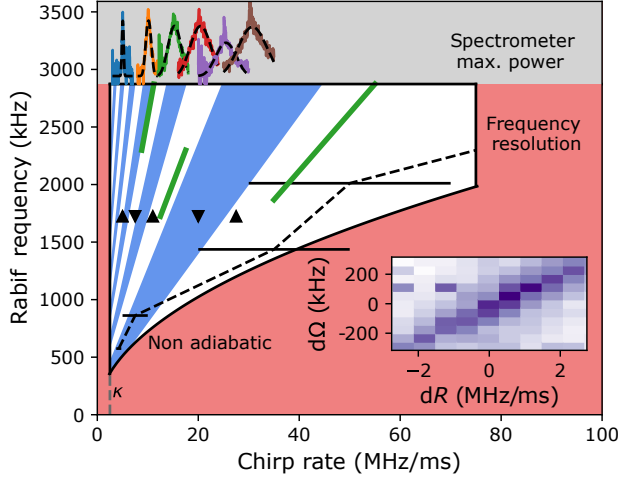


Figure 4. **Counting memory modes.** Each memory mode is determined by the phase pattern ϕ_w imparted by a WURST pulse. The parameter space where WURST pulses efficiently refocus spins is shown bounded in black. Bounds are the cavity linewidth, the maximum spectrometer power and requirements the WURST is adiabatic. A frequency resolution limit occurs due to the homodyne scheme and would be removed in a heterodyne scheme. We measure the adiabaticity limit by thresholding echo intensity shown in the SI and here by the black dashed line giving good agreement with the theoretical line. We measure distinctiveness of WURST pulses using AB-echo sequences. The results of sweeping the B pulse chirp rate at maximum power are inset to the top of the figure and fit by Gaussian profiles. We show a two dimensional map sweeping chirp rate and Rabi frequency in the inset. In 2D sweeps there are lines of WURST pulses which impart the same ϕ_w function to the spin ensemble. Green lines in the main panel show the line of equivalent WURST pulses from other two dimensional maps. Interpolating data from AB-echo sweeps we determine the width of a line of equivalent WURST pulses at fixed Rabi frequency. We partition the space of available WURSTs into unique WURSTs (i.e. memory modes) by constraining neighbouring WURST pulses to be separated by the half width hundredth max and show an example partitioning where blue/white sections indicate unique WURST pulses. We show the WURST pulses used in Fig. 3 where the up/down markers refer to positive/negative chirp direction.

Supplementary Information for Random-access quantum memory using chirped pulse phase encoding

James O'Sullivan,^{1,*} Oscar W. Kennedy,^{1,*} Kamanasish Debnath,² Joseph Alexander,¹
Christoph W. Zollitsch,¹ Mantas Šimėnas,¹ Akel Hashim,³ Christopher N. Thomas,⁴
Stafford Withington,⁴ Irfan Siddiqi,³ Klaus Mølmer,² and John J. L. Morton^{1,5}

¹*London Centre for Nanotechnology, UCL,
17-19 Gordon Street, London, WC1H 0AH, UK*

²*Department of Physics and Astronomy,
Aarhus University, DK-8000 Aarhus C, Denmark*

³*Lawrence Berkeley National Laboratory, Berkeley, CA 94720, USA*

⁴*Cavendish Laboratory, University of Cambridge,
JJ Thomson Ave, Cambridge CB3 0HE, UK*

⁵*Department of Electrical and Electronic Engineering,
UCL, Malet Place, London, WC1E 7JE, UK*

* These authors have contributed equally to this work

I. METHODS

A. Device fabrication

A float-zone silicon wafer of natural isotopic abundance is ion implanted with bismuth at a chain of energies targeting a density of 10^{17} cm^{-3} bismuth in the top $1 \text{ }\mu\text{m}$ of the sample. This is annealed at 900°C for 5 minutes to incorporate the bismuth into the silicon matrix forming spin-active donors. A planar niobium microresonator is patterned on the top of the sample by liftoff. The Nb film is 100 nm thick and has a field dependent frequency (see Ref. [1]) of 7.093 GHz at a magnetic field of 46 mT . A schematic of the device is shown in Fig. S1(a), the simulated bismuth implantation profile in Fig. S1(b) and the simulated microwave magnetic fields caused by the zero point fluctuations in the resonator in Fig. S1(c).

B. Microwave measurement

The measurement setup is shown in Fig. S1(d). The device is mounted inside a copper box which is held at 100 mK on the mixing-chamber plate of a dilution-refrigerator. Two antennae extend into the box; one short stub antenna (high insertion loss $\gtrsim 30 \text{ dB}$, low coupling) is connected to a 30 dB attenuated microwave in-line and used to apply microwave excitations. Another long antenna (large coupling) is used to collect microwave signals and is connected to the amplification chain. The asymmetry results in a large collection efficiency of spin-echo signals. The signal is then routed through two circulators to a Josephson parametric amplifier (JPA), a quantum limited amplifier, which amplifies the signal in reflection. The amplifier is driven via a directional coupler by a dedicated microwave source. Calibration of the JPA is given in the next section. The signal was further amplified at 4 K by a high electron mobility transistor (HEMT) and again at room temperature before being mixed down in frequency by an IQ mixer and detected using a digitiser.

Pulsed microwave signals are generated by an arbitrary waveform generator (AWG), connected to a vector source generator (VSG). These pulses are routed through either a high gain path (solid state amplifier $+35 \text{ dB}$ 3W max output) or an attenuating path (10 dB attenuation) both signal routes are actively gated using fast microwave switches. Signals are routed through the fridge before being mixed down at room temperature.

Continuous wave measurements are performed using a vector network analyser (VNA).

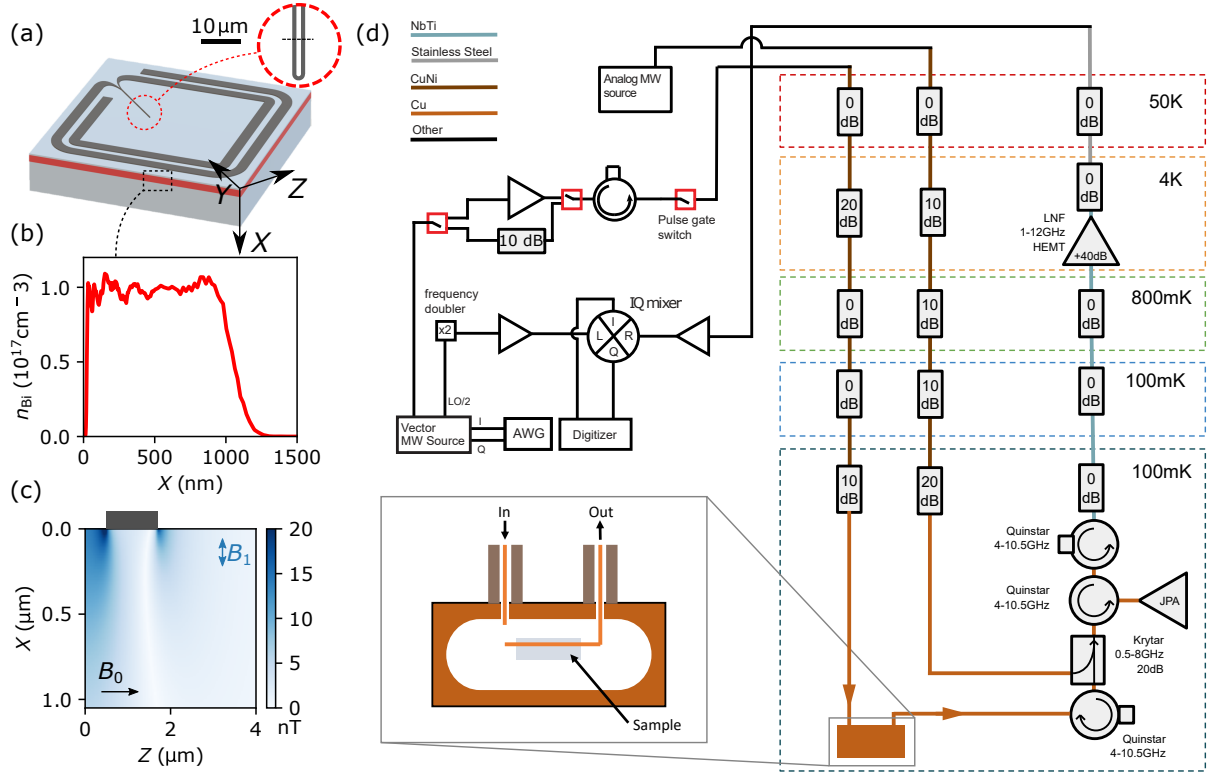


Figure S1. (a) Device schematic showing the double-back inductor. (b) The implanted bismuth profile determined by Monte-Carlo simulations. (c) Finite element modelling of the microwave magnetic field from zero-point fluctuations in the resonator. (d) Schematic of the spectrometer and dilution fridge setup. The copper box housing the cavity is magnified to show the configuration of the sample and antennae inside. The receive antenna is considerably longer than the input antenna to increase coupling to the cavity and maximise signal. Coaxial cable types inside the fridge have been colour coded.

We measured S_{21} transmission between the antennae which is modulated by the microresonator. To characterize the resonator quality factor we fit the modulation (in linear magnitude) with a Breit-Wigner-Fano function:

$$S_{21\text{Lin}}(f) = K \frac{q\kappa/2 + f - f_0}{\kappa^2/4 + (f - f_0)^2} + mx + c \quad (1)$$

where K determines the size of the modulation, q is an asymmetry parameter, f_0 is the central frequency of the resonator, κ is the FWHM of the cavity and the $mx + c$ term is an approximation to the background transmission. This fits our resonance notch well and an example when the resonator is off resonance with the spins is shown in Fig. S2(c)

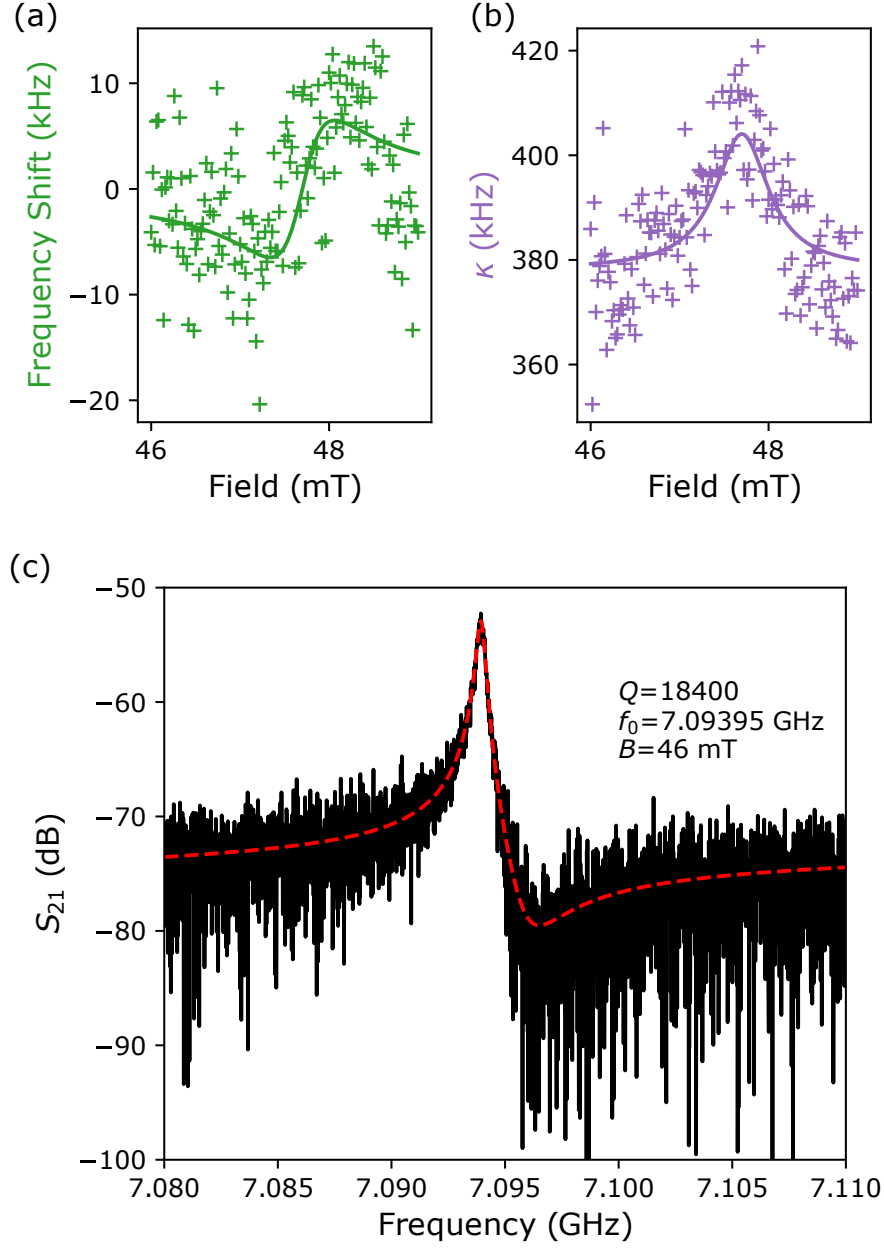


Figure S2. Effect of spins on (a) resonator frequency and (b) resonator linewidth κ as a function of magnetic field as the spin line passes through the resonator. Data are fit simultaneously to equations in Ref. [2] $g_{\text{ens}} \sim 120$ kHz and $\gamma \sim 2.4$ MHz. (c) Measurement of transmission magnitude through the copper cavity using a VNA at 46mT (off resonance with spin line). The superconducting resonator gives a characteristic Fano resonance response which we fit to extract a centre frequency for this resonator of 7.09395 GHz and a Q factor of 18400.

C. System Calibration

We measure T_1 , T_2 and the Rabi frequency of the hybrid system and show these measurements in Fig. I C. T_1 is measured by inversion recovery where the WURST pulse inverts the spin ensemble and we measure the time taken for the inverted ensemble to return to the ground state and find $T_1 \sim 14$ s. T_2 is measured using two WURST pulses to refocus a weak excitation (same strength as in Fig. 2). Varying τ allows us to measure the effect of dephasing on the echo amplitude. We fit a single quadrature of the echo decay returning a coherence time of 0.7(2) ms where most of the uncertainty arises due to different values returned fitting a stretched or single exponential to the data.

To measure the Rabi frequency, Ω , we apply a θ rotation pulse followed 10 ms later by a detection sequence with VSG output power of -20 dBm sent through the high gain path. The θ -pulse is chosen to match the duration and shape of the excitations used in the memory sequence in Fig. 3. The heavily damped envelope to sinusoidal Rabi oscillations (shown in Fig. S3) is due to a large inhomogeneity in single spin coupling, g_0 , across the ensemble. We fit a decaying cosine function to the echo amplitude, allowing us to extract an approximate π pulse amplitude of 0.435 (where 1 is the maximum pulse amplitude at the chosen VSG output power) giving $\Omega = 125$ kHz.

Using T_1 and Ω we calibrate the photon number in the resonator. The Purcell effect limits $1/T_1 = 4g_0^2/\kappa$, allowing a measure of average spin-resonator coupling g_0 . The different κ dependence from Ref. [3] is due to the definition of κ being the HWHM in this work and FWHM in Ref. [3]. At the centre of the line $\kappa \sim 400$ kHz, $T_1 = 14.7$ s giving $g_0 \sim 80$ Hz (g_0 varies across the ensemble and this number is indicative). The Rabi frequency can be written as $\Omega = 2g_0\sqrt{n}$ which allows us to calibrate the photon number $n \sim 5.7 \times 10^5$ for the π pulse above. We can rescale this to the photon number to the memory sequence in Fig. 3 (main text) based on an amplitude of 0.2 at a power ~ 20 dB lower than the Rabi measurement and find $\langle n \rangle \sim 1200$ photons for the memory protocol.

The use of a JPA in measurements was essential to perform experiments at low photon numbers. Such amplifiers are prone to saturation and nonlinearity with large input signals. We calibrate the JPA to determine the onset and extent of the nonlinear regime, and any additional distortions that may be present. For comparison, the same measurements were repeated with the JPA turned off, using only a HEMT at 4 K for amplification. We confirm

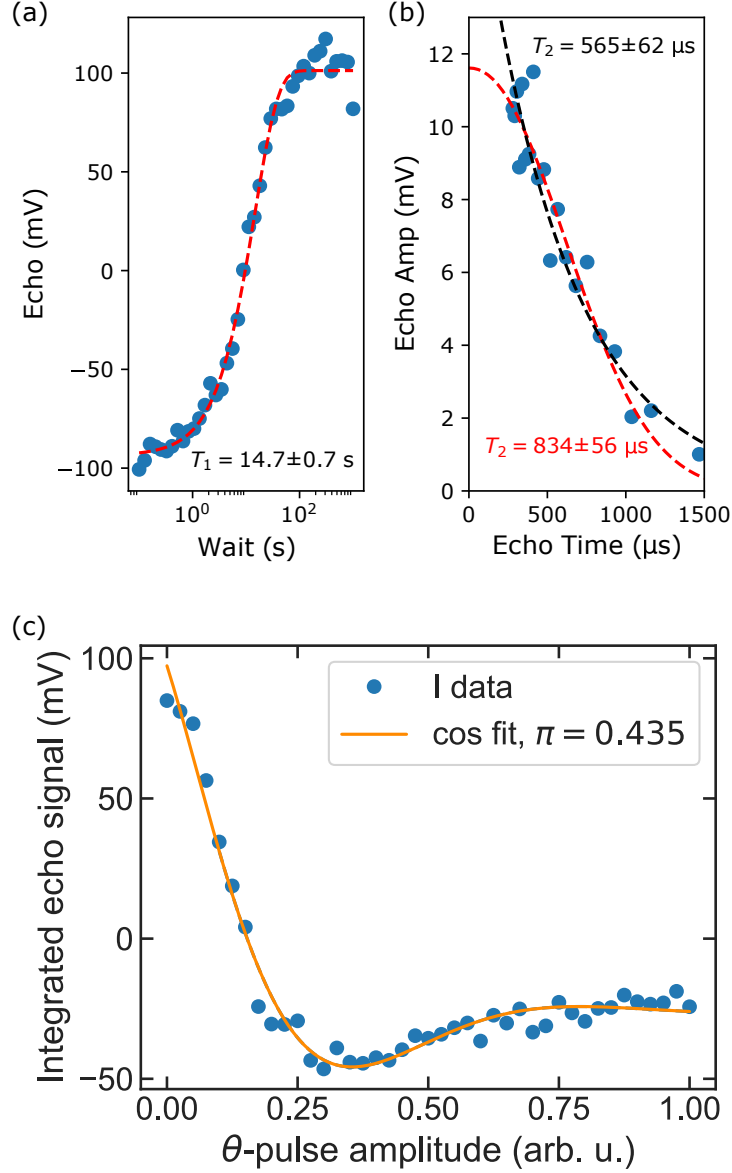


Figure S3. (a) T_1 by inversion recovery. A WURST pulse is used to invert the ensemble before a wait (indicated on the x axis) and a detection sequence at constant high power and τ . (b) T_2 measurement of the sample at the same weak excitation strength as used in Fig. 2 main text. The pulse sequence (inset) is a weak excitation followed by two 100 μ s WURST pulses. Increasing τ changes the echo time allowing T_2 to be measured. Fitting stretched or single exponentials gives different T_2 giving a combined uncertainty of $T_2 = 0.7(2)$ ms (c) Rabi oscillations using a Gaussian θ -pulse of duration 8 μ s and FWHM 4 μ s and a two-WURST silenced echo detection sequence. The oscillations are heavily damped due to a large inhomogeneity in Rabi frequency across the ensemble.

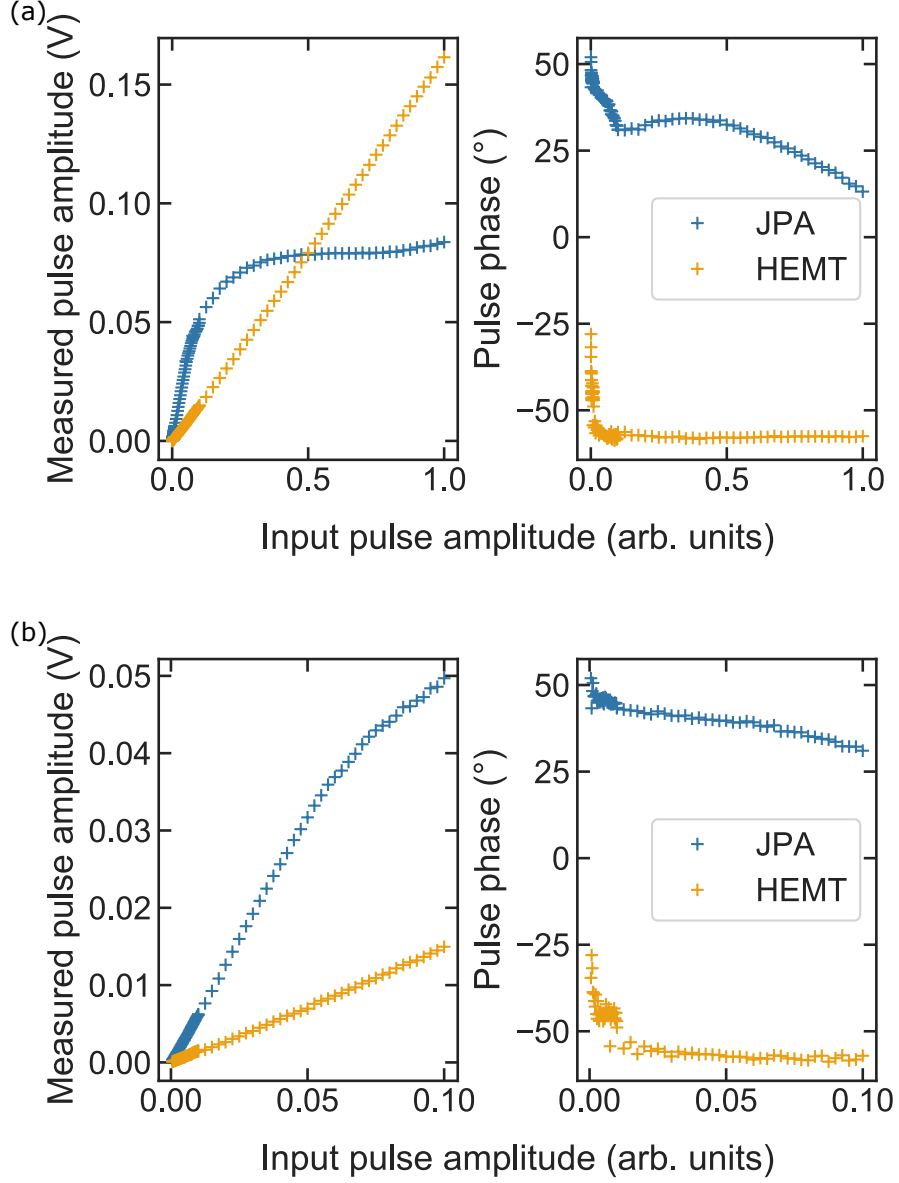


Figure S4. (a) Measured pulse amplitude as a function of input pulse amplitude, measured using the JPA (blue) and the HEMT without JPA (orange). (b) Low power regime of the same experiment.

that for Fig. 3 (main text) the echo signals are well into the linear regime but the input excitations are in the nonlinear regime of the JPA and are prone to distortion. The HEMT remains linear and un-distorted at all powers, as expected. JPA calibrations are shown in Fig. S4.

D. Cooperativity

Cooperativity in a hybrid micro-resonator spin system can be measured by the dispersive shift to the resonator frequency (f), and the increased half-width half max of the resonator frequency response (κ) [2]:

$$f = f_0 - \frac{g_{\text{ens}}^2 \Delta}{\Delta^2 + \gamma^2/4} \quad (2)$$

$$\kappa = \kappa_0 + \frac{g_{\text{ens}}^2 \gamma/2}{\Delta^2 + \gamma^2/4} \quad (3)$$

where κ_0 and f_0 are respectively the half width and frequency of the resonator in the absence of spins, and the detuning $\Delta = (B_0 - B_R) \times \partial f / \partial B_0$, where B_R is the magnetic field at which spins and resonator are resonant. Fitting equations 2 and 3 to our data gives $C \sim 0.067$ as shown in Fig. S2.

We also extract the cooperativity from T_2 measurements with CPMG sequences in Fig. 2 (main text) by modelling the echo intensity as a function of echo number and considering the reduction of energy in the echo field with repeated emission. In A[BB] $_n$ A sequences the echo is emitted after the final A pulse. As (i) WURST pulses efficiently refocus spins and (ii) only one echo forms, we attribute any change in echo intensity to dephasing of the spins. We fit the echo intensity $A_{\text{sil}}(t)$ to extract the dephasing time T_2 using

$$A_{\text{sil}}(t) = \sqrt{A_0^2 \exp(-2t/T_2) + K^2}, \quad (4)$$

where A_0 is the echo amplitude at time $t = 0$, T_2 is the dephasing time and K is the background giving a dephasing time of $T_2 = 2.0 \pm 0.2$ ms for a refocusing rate of 7.1 kHz. We model the echo amplitude in A[AA] $_n$ A sequences by assuming that every time an echo forms, a constant fraction of the energy stored in the echo field is lost and that in between echo emission the echo field dephases as in A[BB] $_n$ A sequences. We model the echo amplitude by

$$A(t) = \sqrt{A_0^2 \exp(-2t/T_2) \times (1 - \eta_{\text{em}})^N + K^2} \quad (5)$$

where η_{em} is the efficiency with which energy is emitted from the echo field to the cavity, N is the number of echoes which have occurred before time t . This is fit with one free parameter, η_{em} , and is shown shown in Fig. 2.

Using Equation (17) from Ref. [4] we relate the one-way efficiency to the cooperativity

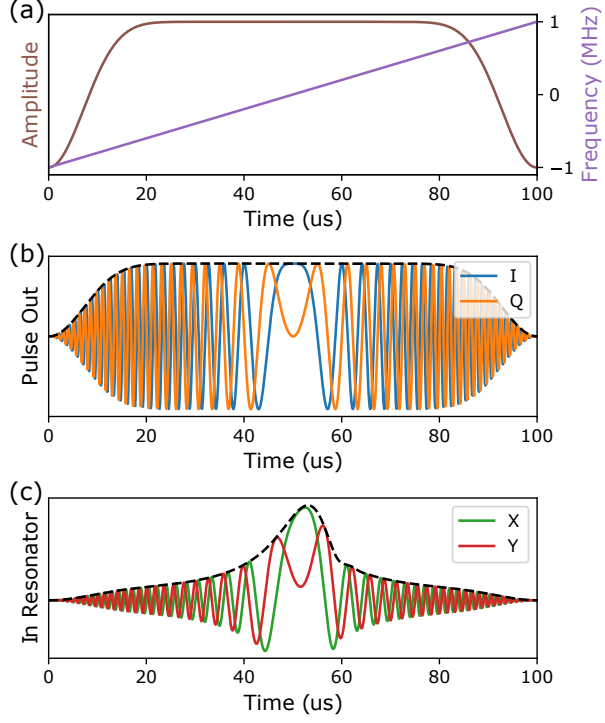


Figure S5. WURST-20 pulses with (a) the pulse amplitude and frequency shift for a WURST pulse with bandwidth 2 MHz and duration 100 μs . (b) The I and Q quadratures of the same WURST pulse. (c) The X and Y field quadratures in the cavity once the WURST pulse is filtered by a $\kappa = 200$ kHz cavity.

by

$$\eta_{\text{em}} = \frac{4C}{(1+C)^2} \quad (6)$$

giving $C = 0.047$ in close agreement to the value extracted in the more typical method by measuring effects on the resonator.

E. WURST Pulses

1. Input Output Theory

Wideband uniform rate smooth truncation (WURST) pulses can be characterized by frequency and amplitude modulation (FM and AM respectively)

$$\begin{aligned} f_W(t) &= -\frac{\Gamma_W}{2} + \frac{\Gamma_W}{T_W}t, \\ A_W(t) &= 1 - \left| \sin\left(\pi \frac{t - T_W/2}{T_W}\right) \right|^N, \end{aligned} \quad (7)$$

where Γ_W is the bandwidth of the WURST pulse, T_W is the WURST pulse duration and N is the WURST pulse index, in this work we use $N = 20$ pulses.

The FM results in a time varying phase of the output pulse

$$\phi(t) = \int_0^t f_W(t') dt' + \phi_0, \quad (8)$$

where ϕ_0 is the phase of the WURST pulse. The I and Q pulse quadratures applied by the AWG are

$$\begin{aligned} I(t) &= A_W(t) \sin \phi(t), \\ Q(t) &= A_W(t) \cos \phi(t), \end{aligned} \quad (9)$$

The WURST pulse is modulated by the cavity described by input/output theory [5, 6] where

$$\begin{aligned} \dot{X}(t) &= \sqrt{\kappa_C} I(t) - \frac{\kappa}{2} X(t), \\ \dot{Y}(t) &= \sqrt{\kappa_C} Q(t) - \frac{\kappa}{2} Y(t), \end{aligned} \quad (10)$$

where κ_C is the coupling linewidth of the cavity and κ is the loaded linewidth of the cavity. Increasing the bandwidth of the WURST pulse above the bandwidth of the cavity shortens the effective WURST pulse duration. We show an example WURST pulse in FM/AM (Fig. S5a), consequent IQ quadratures (Fig. S5b) and after modulation by a cavity (Fig. S5c)

2. Limits on WURST Pulses

In Fig. 4, a region of suitable WURST pulses — WURST pulses which inverts a large fraction of the spin ensemble — is mapped out based on both theory and experiment described in this section. Using pulse sequences such as that in Fig. 1(a) (excitation followed

by two identical WURST pulses) we have measured the refocusing efficiency. We measure the amplitude of the first (nominally silenced) and second echo and present them as a function of the WURST pulse bandwidth and amplitude in Fig. S6. A ‘good’ WURST pulse results in no echo after the first WURST, and a loud echo after the second.

By thresholding the lines we determine regions where WURST pulses adiabatically refocus a large fraction of spins. The constraint that the second echo must have a suitable magnitude (85 mV) gives the experimental boundary to suitable WURST pulses shown in Fig. 4 (main text) based on adiabaticity.

This is supported by a theoretical treatment [7].

$$Q_{\min} = 2\pi\nu^2/R \gg 1, \quad (11)$$

where Q_{\min} is an adiabaticity factor, R is the chirp rate and ν is the nutation frequency (how quickly the spin precesses around the effective field). ν is minimal (and equal to the Rabi frequency) when the WURST frequency is the same as the spin frequency. We choose a minimum g_0 for spins to be refocused and solve this equation for $Q_{\min} = 1$ finding a lower limit on pulse strength.

In the homodyne scheme used in this work there is a limit placed by the finite frequency resolution we can imprint onto WURST pulses. The effective duration of the WURST pulse, $T_{\text{W,eff}} = \kappa T_{\text{W}}/\Gamma_{\text{W}}$, is the time the WURST pulse of duration T_{W} and total bandwidth Γ_{W} takes to chirp across the cavity frequency κ . The inverse of this time gives an indication of the minimum frequency that can be resolved by modulating the pulse. This frequency must be less than the cavity bandwidth placing a limit on the maximum Γ_{W} which can be used,

$$\Gamma_{\text{W}} \ll \kappa^2 T_{\text{W}} = 37 \text{ MHz}. \quad (12)$$

The maximum spectrometer power limits the power of WURSTs we can apply and is shown as the top boundary in Fig. 4. This line cannot be increased to arbitrarily high powers using higher power amplifiers as the superconducting resonators will limit the maximum power. There is also a minimum WURST bandwidth imposed by the cavity bandwidth.

3. WURST pulse distinctiveness

We partition the space of suitable WURSTs into ‘distinct’ WURST pulses to estimate the memory capacity. We partition this region based upon two-WURST echo sequences where

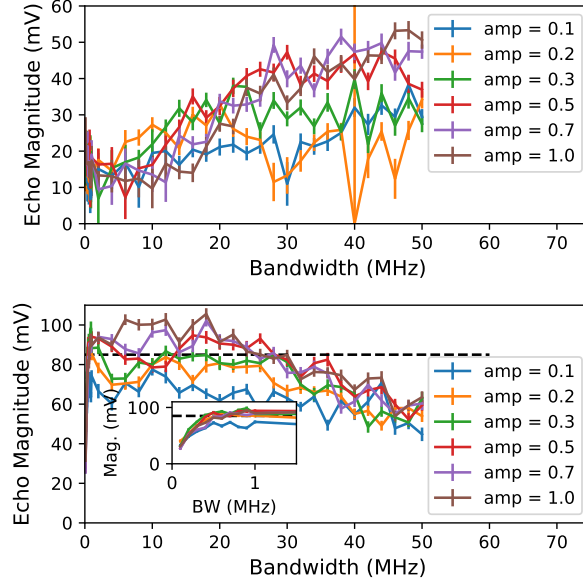


Figure S6. Top (bottom) panel – amplitude of the first (second), nominally silenced (unsilenced), echo as a function of the pulse bandwidth for 200us WURST pulses. Inset to the bottom panel is the unsilenced data for low bandwidths, showing that there is a minimum bandwidth, similar to the cavity width, required to maximise the echo amplitude by refocusing all the spins in the cavity. The adiabaticity limit is determined by thresholding the unsilenced echo intensity relative to 85 mV shown as a black dashed line. Non-monotonicity of echo intensity and uncertainty in echo amplitude give uncertainty in the thresholded value shown in Fig. 4.

the first and second WURST pulse have different properties. Inset to Fig. 4 (main text) is the echo amplitude as the amplitude and chirp rate of the B pulse is varied. This sequence results in strong echoes along a line with positive gradient. In the main text we explain that this line of equivalent pulses is due to the acquisition of a dynamic phase. Together with other two dimensional and one dimensional maps varying a B-pulse parameter we interpolate the gradient and width of the line of equivalent pulses across the space of WURST pulses giving good inversion and use this interpolation to count WURST pulses. This interpolation is shown in Fig. S7 with the results in Fig. 4.

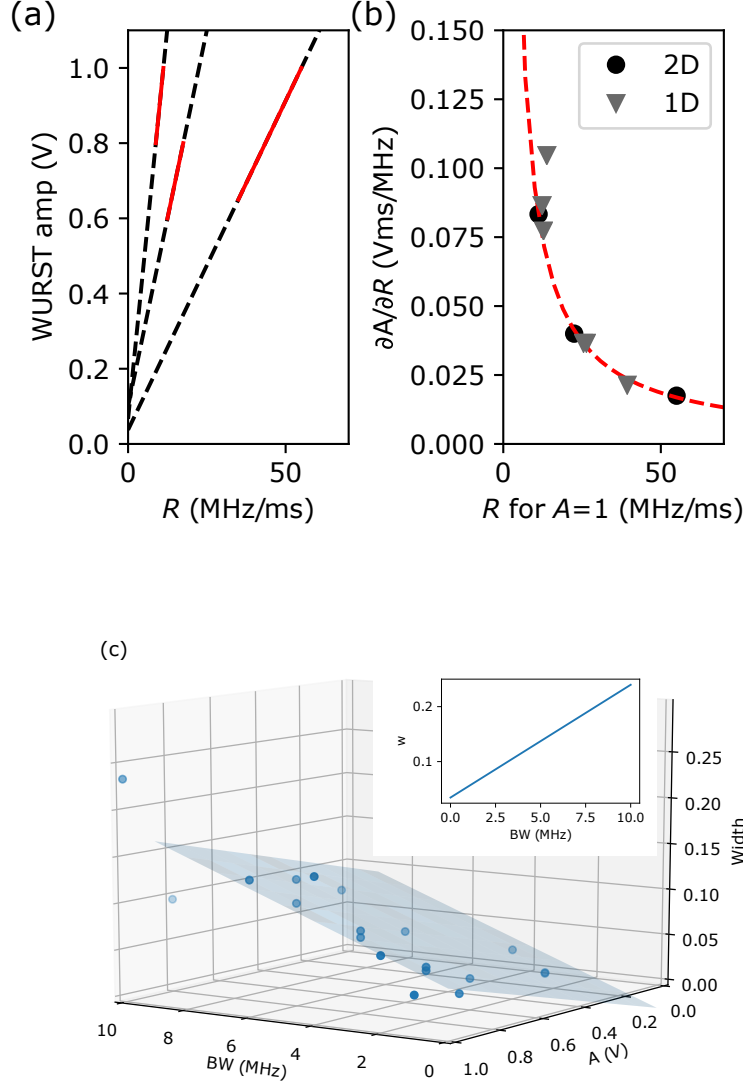


Figure S7. (a) The line of strong echoes from 2D maps of AB-echo sequences. We fit a line to these data and extract their gradient. (b) The gradient of the lines fit in (a) as a function of their extrapolated bandwidth at amplitude $A=1$ (black circles). The gradient determined when B-pulse has been swept in 1D in both amplitude and bandwidth are inferred and plot on the same axes (grey triangles) showing good agreement. We fit these data with $\partial A / \partial R = C / R$ with C a fit parameter and return the red dashed line and $C = 0.93$. (c) Width of the line of equivalent WURST pulses as a function of WURST pulse parameters. We fit a plane to this data to allow interpolation of the width as a function of bandwidth and amplitude.

4. Theoretical description of WURST pulses

The cavity is driven by a chirped field which results in a temporal intensity profile of the field inside the cavity, and the coupled equations for the spins and the cavity field must in general be solved numerically. Here we shall make some observations for a simplified model, that will qualitatively explain most features seen in the experiments. The spins have a central frequency ω_c and each spin is characterized by its detuning $\delta = \omega - \omega_c$. We characterize a WURST pulse by its chirp rate R and pulse centre t_0 , yielding its frequency $\omega(t) = R(t - t_0)$ and phase $\phi(t) = \frac{1}{2}R(t - t_0)^2$ in the frame rotating at ω_c . In that frame the Hamiltonian for each given spin is $\delta\sigma_z/2$, and the time dependent complex Rabi frequency is $\Omega(t) = \Omega_0 \exp(-i\phi(t))$.

The spin transitions are resonant when $R(t - t_0) = \delta$, i.e., at the time $t_\delta \equiv t_0 + \delta/R$. In the interaction picture with respect to the spin excitation energy $\delta\sigma_z/2$, the Hamiltonian of a single spin reads,

$$H_I(t) = \frac{\Omega_0}{2}(e^{-i\phi(t)}e^{i\delta t}\sigma^+ + e^{i\phi(t)}e^{-i\delta t}\sigma^-) \quad (13)$$

where $\phi(t) - \delta t = \frac{1}{2}R(t - t_\delta)^2 + \delta t_0 - \delta^2/2R$.

Assuming a near perfect adiabatic chirp, the unitary evolution operator of the full chirp process is given in the σ_z eigenstate basis:

$$U = \begin{pmatrix} 0 & -ie^{-i\theta_\delta} \\ -ie^{i\theta_\delta} & 0 \end{pmatrix} \quad (14)$$

where $\theta_\delta = \phi_W - \delta t_0$. ϕ_W contains a term $\delta^2/2R$ and a term that does not depend on δ but will in general depend on the chirp rate R and on the coupling strength Ω_0 (see below).

For initial spin states with a (small) excitation amplitude of ϵ at $t = 0$, the δ -dependence of the mean value of the σ^+ operator is $\propto \epsilon e^{2i\delta t_0}$ (disregarding the contribution from ϕ_W), and in the Schrödinger picture, multiplying by $e^{-i\delta t}$ we obtain $\sigma^+ \propto \epsilon e^{i\delta(2t_0 - t)}$. If it was not for the detuning dependence of ϕ_W , these terms would rephase at the time $t = 2t_0$ as in the conventional π -pulse echo. Now, instead, the spins may have very different excitation phases and the integral over δ vanishes and the echo is silenced.

All WURST pulses are described by the same form (14), and the action of two subsequent

pulses (in the interaction picture) at times t_0 and t_1 is readily found,

$$U = U_1 U_0 = \begin{pmatrix} -a^*b & 0 \\ 0 & -ab^* \end{pmatrix} \quad (15)$$

With $a = e^{-i\theta_\delta}$, with parameters R_0, Ω_0 and $b = e^{-i\theta_\delta}$, with parameters R_1, Ω_1 , we get $ab^* = e^{i(\phi_{W_0} - \phi_{W_1}) + i\delta(t_1 - t_0)}$ and if the pulse parameters are identical, this simplifies to $ab^* = e^{i\delta(t_0 - t_1)}$. Thus, after two identical WURST pulses, a weak spin excitation returns with a global minus sign and a detuning dependent phase factor. In the Schrödinger picture, the linear detuning dependence of the phase disappears at $t = 2(t_1 - t_0)$ and we obtain an echo.

Assuming perfect inversion, a sequence with an even number of WURST pulses yields a final phase which is the sum of all WURST phases θ_δ with $+$ ($-$) signs if they are raising (lowering) pulses, cf., (13). Two pulses with different chirp rates or strengths will not cause an echo due to the nontrivial dependence of the phase difference $\phi_{W_0} - \phi_{W_1}$. The quadratic variation $\delta^2(1/2R_0 - 1/2R_1)$ due to the phase chirp may thus cause destructive interference over the distribution of δ and the dynamical phase associated with the energies of the adiabatic eigenstates during the chirped adiabatic process may cause destructive interference over a range of values for the coupling strength.

As we observe in the experiments, variation of the chirp rate and strength permit addressing of separate storage modes. The field amplitude Ω_0 , and the chirp rate R both appear in the dressed state energies and hence in the dynamical phases, and the two control parameters turn out not lead to exploration of a two dimensional space of storage modes. An analytical theory for the phase textures indicated in Fig.1(b) would require solution of the driven two-level dynamics by a chirped frequency field with a time and frequency dependent Rabi frequency $\Omega_0(t)$ imposed by the finite bandwidth cavity mode. While this is not possible, we can solve the dynamics numerically and verify the various contribution to the phases and their constructive interference over the spin ensembles. By discretizing an inhomogeneously broadened spin ensemble into 100,000 subensembles and solving their individual dynamics subject to chirped pulses, we obtain the value of $\langle \sigma_y \rangle$, summed over all the spins, shown in the Fig S8. Two weak pulses are stored in the spins as indicated by the red circles. The timing of the A, B, B and A pulses then ensures the early echo of the second and the later echo of the first pulse (blue arrows) and the calculation confirms the

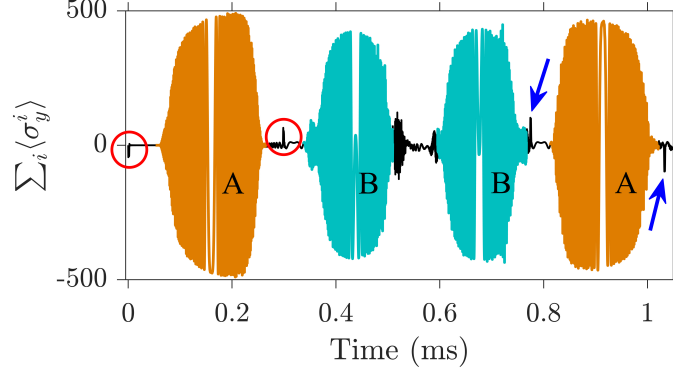


Figure S8. (a) Retrieval of two weak excitations within an ABBA sequence of WURST pulses with different chirp rates, $R_A = -2\pi \times 11.25$ MHz/ms and $R_B = 2\pi \times 7.50$ MHz/ms. The pulses explore the same finite frequency interval and have the same amplitude.

functioning of the scheme described in the main text.

F. First In Fast Out

In Fig. S9 we show how using pairs of WURST pulses we can store and retrieve trains of excitations. In Fig. S9(a) we show the experimental data where the phase of the excitations and echoes allows them to be mathed up before and after the WURST pulses. In Fig. S9(b) we show the phase evolution as in Fig. 1 main text, explaining why this realises a first in first out (FIFO) memory which allows states to be retrieve in the order they were stored. This can be used in the memory protocol shown in Fig. 3 (main text) to extend the capacity of the memory as each distinct mode can strings of multiple excitations which can be retrieved.

G. High power memory sequences

To further confirm the memory protocol functions as intended, we ran identical memory protocols cycling different excitations on and off so that in each run only one excitation was used. To speed up this measurement we increased the power of the input pulses and the results are shown in Fig. IG where we also show a replication of the full memory protocol at higher power. In each of the sequences where there is only one excitation stored, we only retrieve one echo, and the echo occurs when we would expect the echo to form further

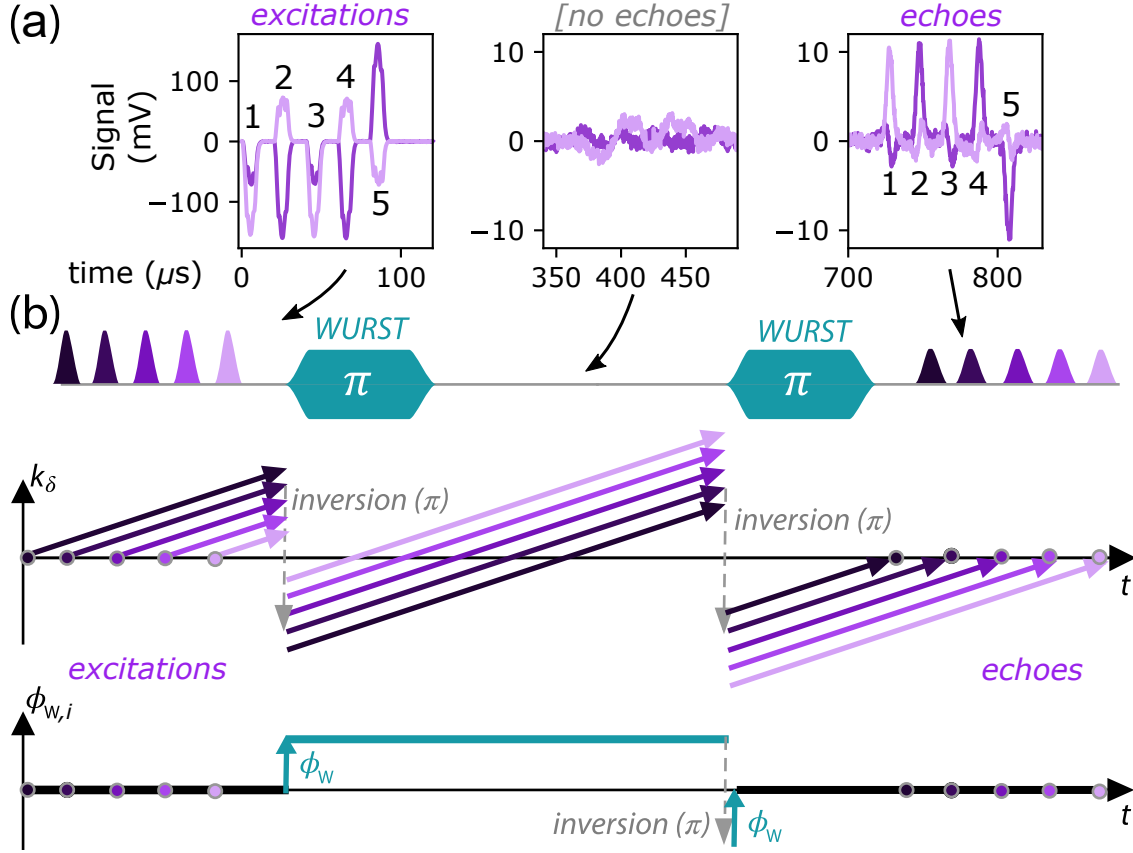


Figure S9. First in first out (FIFO) time bin encoding of multiple echoes. (a) An experimental demonstration of multiple excitations stored in FIFO protocol with WURST pulses. The pattern of excitation/echo phases allows echoes and excitations to be paired. (b) schematic showing evolution of spin waves and WURST phase resulting in the FIFO encoding with silenced excited echoes.

confirming that the memory protocol works.

-
- [1] James O'Sullivan, Oscar W Kennedy, Christoph W Zollitsch, Mantas Šimėnas, Christopher N Thomas, Leonid V Abdurakhimov, Stafford Withington, and John JL Morton. Spin-resonance linewidths of bismuth donors in silicon coupled to planar microresonators. *Physical Review Applied*, 14(6):064050, 2020.
 - [2] Eisuke Abe, Hua Wu, Arzhang Ardavan, and John J. L. Morton. Electron spin ensemble strongly coupled to a three-dimensional microwave cavity. *Applied Physics Letters*, 98(25):251108, 2011.

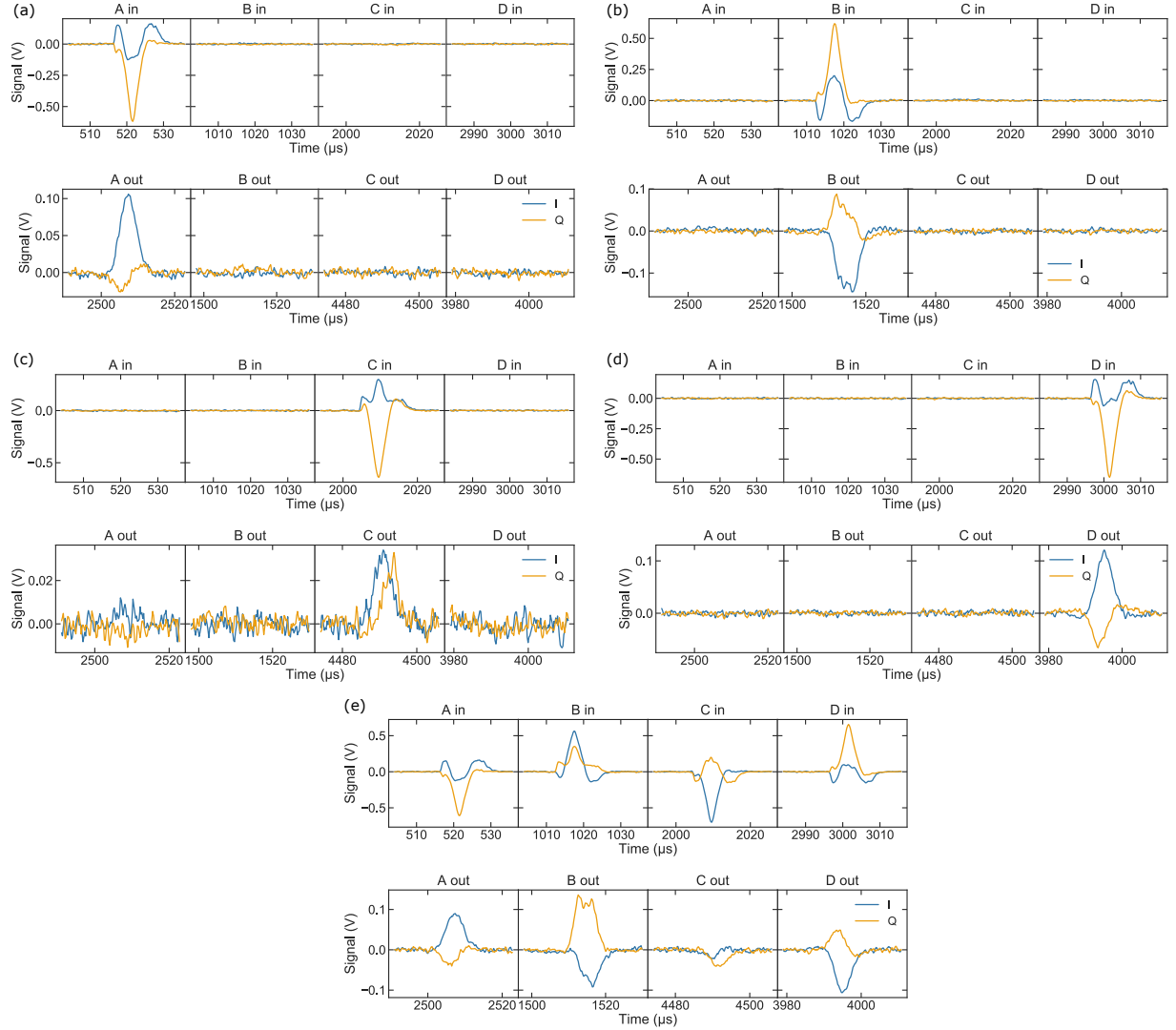


Figure S10. The memory sequence shown in Fig.3 was performed at higher input power (~ 15000 photons per excitation pulse); the raw transient trace of the sequence is shown in (e). In Figs.(a-d) the same experiment was repeated with only one of each of the 4 input excitation pulses, A,B,C and D turned on. This allows us to unambiguously determine which echo originates from which excitation pulse. We see that a single echo appears in the expected read slot in each case. We also see that no other echoes appear when only one excitation is turned on. In this power regime, as well as amplifying (non-linearly), the JPA also imparts poorly characterized phase shifts seen particularly when comparing (c,d,e).

- [3] Audrey Bienfait, JJ Pla, Yuimaru Kubo, Xin Zhou, Michael Stern, CC Lo, CD Weis, Thomas Schenkel, Denis Vion, Daniel Esteve, et al. Controlling spin relaxation with a cavity. *Nature*, 531(7592):74–77, 2016.
- [4] Mikael Afzelius, N Sangouard, Göran Johansson, MU Staudt, and CM Wilson. Proposal for a coherent quantum memory for propagating microwave photons. *New Journal of Physics*, 15(6):065008, 2013.
- [5] Crispin W Gardiner and Matthew J Collett. Input and output in damped quantum systems: Quantum stochastic differential equations and the master equation. *Physical Review A*, 31(6):3761, 1985.
- [6] Vishal Ranjan, Sebastian Probst, Bartolo Albanese, Andrin Doll, Oscar Jacquot, Emmanuel Flurin, Reinier Heeres, Denis Vion, Daniel Esteve, JJL Morton, et al. Pulsed electron spin resonance spectroscopy in the purcell regime. *Journal of Magnetic Resonance*, 310:106662, 2020.
- [7] Andrin Doll, Stephan Pribitzer, René Tschaggelar, and Gunnar Jeschke. Adiabatic and fast passage ultra-wideband inversion in pulsed EPR. *Journal of Magnetic Resonance*, 230:27–39, 2013.